Title: Antigen-presenting fibroblasts sustain anti-tumour CD4$^+$ T cells in situ via MHCIIp-TCR and C1q-C1qbp binding.

Authors: [1]Dimitra Kerdidani, [1]Katerina Goudevenou, [1]Emmanouil Aerakis, [1]Kleio-Maria Verrou, [1]Petros Stamoulis, [1]Christos Tzaferis, [1]Alejandro Prados, [2]Georgios Vamvakaris, [3]Evangelos Kaniaris, [4]Konstantinos Vachlas, [4]Evangelos Sepsas, [4]Konstantinos Potaris, [5]Anastasios Koutsopoulos and [1]Maria Tsoumakidou*.

Affiliations:

[1]Institute of Bioinnovation, Biomedical Sciences Research Center "Alexander Fleming", Vari, Greece

[2]Department of Pathology, Sotiria Chest Hospital, Athens, Greece

[3]Department of Respiratory Medicine, Sotiria Chest Hospital, Athens, Greece

[4]Department of Thoracic Surgery, Sotiria Chest Hospital, Athens, Greece

[5]Department of Pathology, Medical School, University of Crete, Greece.

Running title: MHCII fibroblasts sustain T cells within tumours.

Keywords: fibroblasts, tumours, MHCII, CD4 T cells

Corresponding author: Maria Tsoumakidou, Institute of Bioinnovation, BSRC "Alexander Fleming", Greece, 16672. Phone:(167)+30-210-9653310; Fax: +30-210-9653934; E-mail: tsoumakidou@fleming.gr

Author contributions: Conception and design study, M.T.; Development of methodology, M.T.; Acquisition of data, D.K., K.G., E.A., P.S., A.P. and M.T.; Analysis and interpretation of data, D.K., K.M.V., C.T., and M.T.; Providing human samples, G.V., E.K., K.V. E.S., K.P. and A.K.; Writing the manuscript, M.T.; Preparing the figures, D.K.; Study supervision, M.T.

Disclosure of potential conflict of interest: None

Manuscript notes: 9.867 words, 5 main figures, 10 supplementary figures and 2 supplementary tables

ABSTRACT

In situ antigen presentation is required to sustain active proliferating $CD4^+$ T cells in tumours and to help form memory $CD8^+$ T cells, but the antigen presenting cells (APCs) and pathways involved remain elusive. Cancer associated fibroblasts (CAFs) are prominent stromal constituent of solid tumors. Current immunological dogma considers that CAFs facilitate tumour immune escape. A new subset of MHCII antigen presenting cancer-associated fibroblasts (apCAFs) has been described, but their function remains unknown. Here we report a previously unrecognized function of apCAFs in sustaining $CD4^+$ T cells in primary human and murine lung tumours. In response to IFNγ and oxidative stress in tumours CAFs up-regulated MHCII. Fibroblast-specific targeted ablation of MHCII induced a hypometabolic hypoproliferative state in $CD4^+$ T cells, which impacted MHCII and MHCI immunity, accelerating tumor growth. apCAFs directly presented MHCII-peptide (MCHIIp) complexes to activate the TCRs of $CD4^+$ T cell. Highthrough-put profiling and blocking assays unveiled a novel CAF to T cell communication pathway via complement 1q binding on membrane C1qbp. Thus, apCAFs sustain anti-tumor $CD4^+$ T cells via MHCIIp-TCR and C1q-C1qbp binding. Our studies pave the way to the design of novel immunotherapeutic strategies that will harness apCAFs to help sustain T cells inside solid tumours.

Statement of significance

This work challenges the immunological dogma that dominant physiological significance in tumour specific immunity comes only through professional APCs, leading to the design of novel MHCII fibroblast-directed strategies to sustain endogenous or adoptively transferred $CD4^+$ T cells within solid tumors.

INTRODUCTION

Despite the past extensive focus on $CD8^+$ T cells, effective priming of tumor antigen-specific $CD4^+$ T cells turns out to be of paramount importance for tumor immunity and response to immunotherapy[1-3]. $CD4^+$ T cells help the induction of cytolytic and memory $CD8^+$ T cells[4,5] and can be programmed to cytotoxic cells with direct killing activity[6]. Antigen-inexperienced (naïve) T cells are primed in tumor draining lymph nodes (TudLNs) after direct contact with resident conventional dendritic cells (cDCs) presenting antigens they have acquired from migratory cDCs[7]. Upon encountering antigen, naïve cells proliferate and become activated effector cells that egress from TudLNs and enter tumours. In situ antigen presentation is required to retain T cells in peripheral tissues, including tumours and to establish memory[8-11], but the antigen presenting cells (APCs) and pathways involved are incompletely understood. Although several cells can be induced to express MHCII, only professional APCs, mainly cDCs, constitutively express MHCII, can present MHCII-peptide (MHCIIp) complexes and at the same time provide co-stimulatory molecules for full activation[12]. It has been assumed, albeit not convincingly shown, that further to transferring antigens to TudLNs, intratumoral cDCs help sustain an active and proliferating T effector cell pool in situ.

Cancer associated fibroblasts (CAFs) are prominent stromal constituent of many solid tumors. It has been long considered that CAFs facilitate cancer progression by fueling cancer cell proliferation, angiogenesis, metastasis, and by creating an immunosuppressive inflammatory microenvironment that abrogates the function of adaptive immune cells and facilitates tumour escape[13]. This was challenged by the discovery of CAF heterogeneity and distinct populations that can confer positive clinical outcomes[14-16]. Positive effects of CAFs on T cell immunity have been found to be chemokine mediated and antigen unspecific[14]. A new subset of MHCII-expressing cancer-associated fibroblasts was just discovered in pancreatic adenocarcinoma[17] and in breast carcinoma (bioRxiv, doi.org/10.1101/2020.01.12.903039), but their function remains unknown[17]. Due to the lack of co-stimulatory molecules, it has been hypothesized that antigen-presenting CAFs (apCAFs) induce $CD4^+$ T cells anergy or differentiation into Tregs[17].

Here we report a previously unrecognized function of fibroblasts in sustaining $CD4^+$ T cells in primary human and murine lung tumours. In response to IFNγ and oxidative stress in the tumour microenvironment CAFs up-regulated MHCII. Fibroblast-specific targeted ablation of MHCII induced a hypometabolic hypoproliferative state in tumor-infiltrating $CD4^+$ T cells, which impacted MHC class II and class I immunity, accelerating lung tumor growth. Primary human CAFs directly presented MHCII-peptide (MCHIIp) complexes to activate the TCRs of autologous intratumoral $CD4^+$ T cell, which was recapitulated in murine CAFs and shown to be specific for an MHCII-restricted cancer epitope. Unbiased single cell RNA-seq and ex-vivo assays unveiled a novel inter-cellular communication pathway between primary human CAFs and $CD4^+$ T cells via complement 1 q (C1q) binding on C1qbp on the surface of T cells. These results show that antigen presenting fibroblasts are key APCs sustaining locally anti-tumor $CD4^+$ T cells

via MHCIIp-TCR and C1q-C1qbp binding and therefore need to be considered when designing immunotherapeutic strategies to sustain the pool of endogenous and/or adoptively transferred cancer antigen-specific T cells.

RESULTS

MHC class II expression by CAFs in primary human lung adenocarcinomas and squamous cell carcinomas

Effective $CD4^+$ T cell tumor immunity requires that MHCII cancer antigens are presented locally in tumors[1]. We undertook a pilot analysis of MHCII expression in human lung adenocarcinomas (LUAD) and squamous cell carcinomas (LUSQ) by immunohistochemistry. We noticed scattered niches of $MHCII^+$ fibroblast-like cells preferentially located inside the tumor bed relatively to tumor-free lungs (Figure 1a). We elaborated further on the fibroblastic identity of these cells. Immunofluorescence microscopy revealed MHCII expression by intratumoral Fibroblast Activation Protein alpha $(FAP\text{-}\alpha)^+$ cells (Figure 1b). To analyze co-expression of known mesenchymal markers at the single cell level we proceeded to FACS analysis of human lung carcinomas and plotted $HLA\text{-}DR^+$ fibroblasts, gated as FS^{high} non-haematopoietic, non-epithelial, non-cancer, non-endothelial cells ($CD45^-CD31^-$Pan-$cytokeratin^-EPCAM^-$) on t-SNE plots. $HLA\text{-}DR^+$ CAFs co-expressed FAP and PDGFRa, while Podoplanin, Vimentin and CD29, but not aSMA were expressed at variable levels (Figures 1c, 1d). Thus, we convincingly identified apCAFs in primary human lung carcinomas.

Induction of MHC class II in fibroblasts by tumour-derived IFNγ and oxidative stress

The preferential distribution of $MHCII^+$ fibroblast-like cells in tumors rather than tumor-free lungs suggested that the tumor microenvironment (TME) induces MHCII expression in CAFs. We compared MHCII expression by primary human lung CAFs versus paired fibroblasts from macroscopically tumor-free lungs. We found that fewer lung fibroblasts expressed HLA-DR compared to CAFs (Figure 2a). To validate further these findings, we applied two models of orthotopic lung cancer and one model of metastatic cancer. We inoculated one commercially available ($LLC^{mCherry}$) or an autochthonous cancer cell line ($CULA^{mCherry}$) in the left lung lobe of syngeneic mice or injected melanoma cells (B16F10) in the tail vein of mice. Murine $MHCII^+$ FS^{high} non-haematopoietic ($CD45^-$), non-epithelial ($EPCAM^-$), non-endothelial ($CD31^-$), non-cancer cells ($mCherry^-$) plotted on t-SNE plots ubiquitously expressed vimentin, revealing their mesenchymal identity. The CAF markers FAP, PDGFRa and podoplanin were also expressed, albeit by a smaller percentage of cells (Supplementary Figure 1). Confocal microscopy confirmed the existence of intratumoral $MHCII^+Podoplanin^+$ cells (Figure 2b).

FIGURE 1

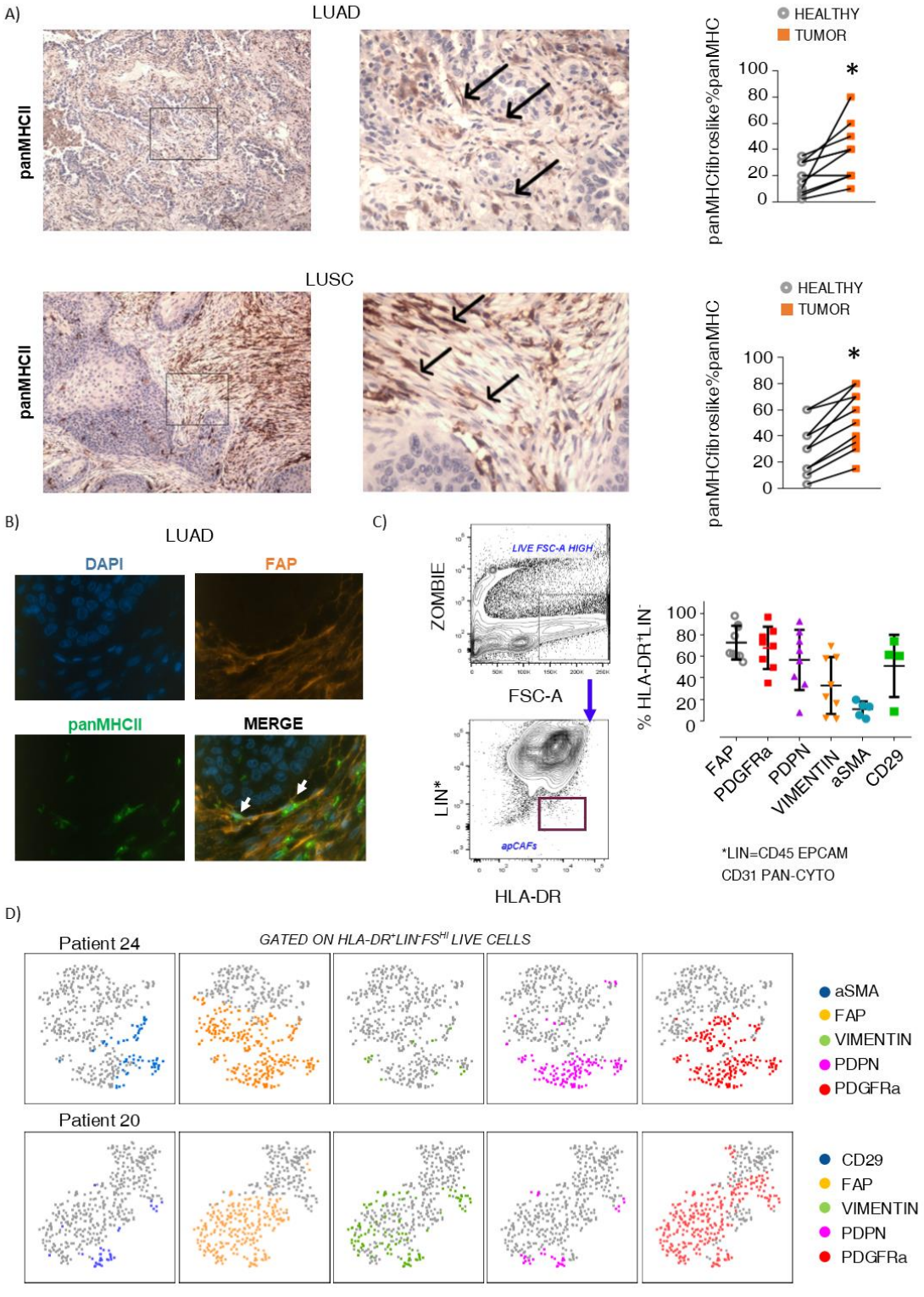

Figure 1. CAFs in human lung adenocarcinomas and squamous cell carcinomas express MHC class II.

A) *Representative images and standardized enumeration from immunohistochemistry (IHC) stainings of*

tumour sections from human lung adenocarcinoma (n=10 patients) (top) and squamous cell carcinoma (n=10 patients) (bottom), using panMHC antibodies. Arrows are pointing to examples of CAFs. ***B)*** *Representative image from an immunofluorescence (IF) staining of a human lung adenocarcinoma section, using panMHCII and FAP antibodies. Arrows are pointing to examples of MHCII^{+} CAFs.* ***C)*** *Left: Representative FACS analysis of a digested lung tumor. Forward-scatter was used to eliminate small-sized cells and Zombie staining to eliminate dead cells. CD45 was used as an immune cell marker, EpCAM and pancytokeratin as epithelial/cancer cell markers and CD31 as endothelial cell marker. Cells that were negative for all the above and positive for HLA-DR (purple rectangle) were gated for expression of fibroblast markers. Right: Cumulative data from 4-9 different patients.* ***D)*** *t-SNE plots with flow cytometry data showing co-expression scheme of fibroblast markers in human HLA-DR^{+}CD45^{-}Epcam^{-}PanCyt^{-}CD31^{-} FS^{hi} lung tumor cells. Two representative patients are shown.*

Similar to what we had observed in humans, MHCII was more frequently expressed by CAFs relatively to healthy lung fibroblasts in all three mouse models (Figure 2c). To corroborate that the TME induced MHCII in CAFs, we developed an in vitro model system where we sorted PDGFRa^{+}Podoplanin^{+} CAFs and cultured them in 3D conditions in Matrigel. Although by day 3 all cultured CAFs had lost MHCII, exposure to fresh lung tumor, but not to healthy lung homogenates, restored MHCII expression at in vivo levels (Figure 2d). MHC-II expression can be induced in most cell types and tissues by IFN-γ. MHCII was slightly decreased in CAFs of IL12p35-/- and IL12p40-/- mice compared to those of WT mice and almost diminished in CAFs of IFNγR-/- and IFNγ-/- mice (Figure 2e). Accordingly, exposing primary cultured CAFs to rIFNγ partly restored lost MHCII expression (Figure 2f). Because neutralizing IFNγ in tumor homogenates could not completely abrogate MHCII induction in vitro, we suspected that that other stimuli acted in parallel to IFNγ to induce MHCII in CAFs. Oxidants accumulate in the TME, can induce MHCII and also epigenetically regulate IFN-γ mediated MHCII[18,19]. Adding anti-oxidants to tumour homogenates largely suppressed MHCII expression in CAFs (Figure 2f). These data collectively suggest that IFNγ and oxidative stress act simultaneously to up-regulate MHCII in CAFs.

FIGURE 2

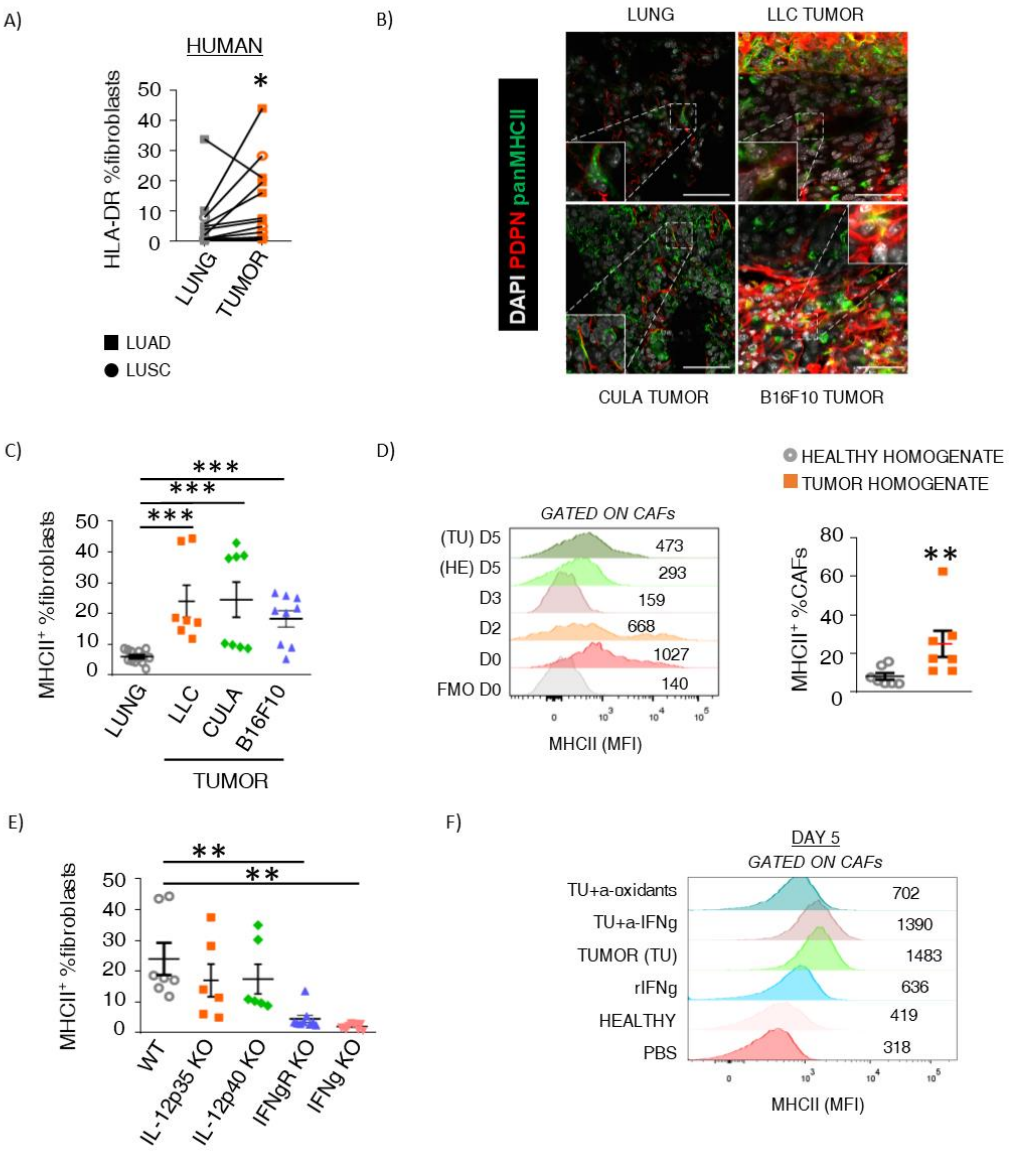

Figure 2: MHC class II expression in CAFs is induced by IFNγ and oxidative stimuli in the TME. A) *Quantitative FACS data on MHCII expression in fibroblasts ($FS^{hi}Lin^{-}FAP^{+}PDGFRa^{+}$) of paired human lung tumors and tumor-free lungs (Wilcoxon test). Circles represent lung adenocarcinoma patients (n=7). Rectangles represent squamous cell carcinoma patients (n=6).* ***B)*** *IF of Podoplanin and MHCII on healthy lung, LLC lung tumour, CULA lung tumour and lung metastasis from B16F10 melanoma. Confocal Imaging. Scale bar, 50μm.* ***C)*** *Quantitative FACS data on MHCII expression in fibroblasts ($FS^{hi}Lin^{-}PDGFRa^{+}$) of murine LLC, CULA and B16 lung tumors and from healthy lungs (n = 7-10 per group from 2 experiments, Mann-Whitney test).* ***D)*** *$PDGFRa^{+}$ CAFs were isolated from LLC lung tumors. Sorted cells were cultured 3D in Matrigel. On day 4 Matrigel was supplemented with homogenate of LLC lung tumor*

or healthy lung. Fibroblasts were analyzed at different time points by FACS for MHCII expression. Representative FACS histogram plots. Quantification is shown on the right (n=7 from 4 experiments). ***E)*** *Cumulative MHC class II expression on fibroblasts ($FS^{hi}Lin^{-}PDGFRa^{+}$) from naive B6.WT, B6. IL12p35-/-, B6.IL12p40-/-, B6.FNγR-/- and B6.IFNγ-/- mice (n = 3-5 per group from 2 experiments, Mann-Whitney test).* ***F)*** *Representative FACS histogram plots from the CAF 3D culture assay as in D, but with CAFs exposed to recombinant IFNγ or tumor homogenates plus/minus anti-oxidants or a-IFNγ (n=2-3 experiments).*

Tumor escape upon targeted deletion of MHCII in fibroblasts

We asked whether MHC class II expression by CAFs was a bystander, suppressor or driver of tumor progression. We set up pilot experiments starting with three murine lines expressing Cre recombinase (Cre) driven off Twist[20], collagene VI[21], and collagen 1a2 (Col1a2) promoters[22], which are lineage markers for mesenchymal cells. Lineage-restricted expression in $LLC^{mCherry}$ lung tumors was determined by Cre-driven GFP expression. An important fraction of intratumoral Twist-driven GFP expressing cells were $CD45^{+}$ cells consistent with cells of the haematopoietic lineage, while Collagene VI-driven GFP-expressing cells could not be identified in lung tumors (Supplementary Figure 2). Col1a2-driven GFP-expressing cells in lung tumors of Col1a2-CreER mice were $CD45^{-}CD31^{-}EPCAM^{-}$ and largely FAP^{+}, $PDGFRa^{+}$, $Podoplanin^{+}$ - indicating that they were bona fide CAFs-, while about half of GFP^{+} cells expressed MHCII (Figure 3a). Thus, the Col1a2-CreER mouse strain is highly specific for targeting lung CAFs including, but not limited to apCAFs. Confocal microscopy confirmed MHCII-GFP co-expression (Figure 3b). Therefore, we used Col1a2-CreER mice for our subsequent studies. $I\text{-}A^{b}$ is the MHC class II molecule expressed in B6 mice and its expression can be deleted from Cre-expressing cell lineages using a floxed I-Ab gene ($I\text{-}A^{b\text{-}fl/fl}$)[23]. We inoculated $LLC^{mCherry}$ cells that expressed the model antigen ovalbumin (ova) in the lungs of Col1a2 $CreER^{+}$I-Ab-$^{fl/fl}$ and Col1a2 $CreER^{-}$I-Ab-$^{fl/fl}$ mice. We found that MHCII expression was significantly decreased, albeit not completely abolished, in CAFs of Col1a2 $CreER^{+}$I-Ab-$^{fl/fl}$ mice (Figure 3c). Despite partial MHCII deletion in CAFs, lung tumor burden was increased and tumors appeared immunologically colder, with fewer $CD4^{+}$ T cell, $CD8^{+}$ T cell and B cells (Figure 3d). Furthermore, Ova peptide-MHCI tetramers stained less of $CD8^{+}$ T cells in lung tumors of Col1a2 $CreER^{+}$I-Ab-$^{fl/fl}$ versus Col1a2 $CreER^{-}$I-Ab-$^{fl/fl}$ mice (Figure 3d). Importantly, $CD8^{+}$ T cell-depleting antibodies abolished differences in tumor burden between Col1a2 $CreER^{+}$I-Ab-$^{fl/fl}$ and Col1a2 $CreER^{+}$I-Ab-$^{fl/fl}$ mice, indicating that the anti-tumour functions of I-Ab (MHCII) were strongly dependent on $CD8^{+}$ T cells (Figure 3e). We questioned whether MHCII-expressing CAFs were sufficient to sustain $CD4^{+}$ and $CD8^{+}$ T cells in the absence of continuous T cell migration from TudLNs. Therefore, we treated mice with a S1PR antagonist FTY720, which blocks egress of T cells from TudLNs, for 5 consecutive days, starting on day 7 after OVA-LLC transplantation[24].

$CD4^+$ and $CD8^+$ T cells were still decreased, while ova peptide-MHCI tetramers still stained less of $CD8^+$ T cells in lung OVA-LLC tumors of FTY720-treated MHCII conditional knockout mice (Figure 3f). These results convincingly show that targeting MHCII expression in CAFs facilitates tumour escape by acting locally.

Lymph node fibroblastic reticular cells (FRCs) have contradictory roles in immune responses, such as inhibition of T cell proliferation via nitric oxide[25] and T cell reprogramming towards memory T cells via IL6[26]. Albeit FRCs in TudLNs acquire transcriptional programs typically associated with tumor escape[12], we considered the possibility that immune evasion in Col1a2 Cre^+I-$A^{b\text{-}fl/fl}$ mice resulted from MHCII deletion in FRCs. We examined MHCII expression in TudLN FRCs by Cre-driven GFP expression. A minor percentage of $CD45^-EPCAM^-CD31^-podoplanin^+$ cells (FRCs) expressed GFP (Supplementary Figure 3a). We also assessed MHCII expression in TudLN FRCs of Col1a2 $CreER^+$I-Ab-$^{fl/fl}$ versus Col1a2 $CreER^-$ I-Ab-$^{fl/fl}$ mice and found only a trend toward decreased $MHCII^+$ FRCs (Supplementary Figure 3b). Furthermore, there were no gross differences in nodal $CD4^+$, $CD8^+$ T cells and B cells (Supplementary Figure 3c). Taking together with the failure of FTY720 treatment to abrogate the immunological outcomes of MHCII deletion in Col1a2 expressing cells, these results strongly suggest that tumor escape in Col1a2 Cre^+I-$A^{b\text{-}fl/fl}$ mice is primarily driven by MHCII loss in CAFs rather than in FRCs.

CAF MHCIIp-TCR binding maintains metabolically active proliferating anti-tumour $CD4^+$ T effector cells

Targeting MHCII antigen presentation is expected to primarily impact $CD4^+$ T cells. Differential expression analysis of bulk intratumoral $CD4^+$ T cell RNA sequencing data showed a remarkable number of down regulated genes in MHCII conditional knockout mice (Figure 4a). Among top 10 were genes involved in mitochondrial (Cyb5b, Atp5g1, Crem, Lipa) and ribosomal metabolic possesses (Prpf4b, Wbp4, Zc3h11a) (Figure 4a, Supplementary Figure 4a). Down-regulation of these genes was confirmed by RT-PCR in distinct cohorts of mice (Supplementary Figure 4b). Likewise, comparing top 10 pathway activities of downregulated genes in $CD4^+$ T cells of Col1a2 $CreER^+$I-Ab-$^{fl/fl}$ versus those Col1a2 $CreER^-$I-Ab-$^{fl/fl}$ mice, showed enrichment in metabolic processes, such as protein catabolism, ribosome biogenesis, mRNA processing (Figure 4b). The strength of TCR activation is critical for the bioenergetics of T cells[27], suggesting that deleting MHCII from CAFs deprived intratumoral $CD4^+$ T cells from TCR binding. To test this, we sorted CAFs from OVA-$LLC^{mCherry}$ versus $LLC^{mCherry}$ tumors and co-cultured them with OVA-specific $CD4^+$ T effector cells from OTII mice. The first stage of the TCR signaling cascade after MHCp-TCR binding is the phosphorylation of the CD3ζ subunits of the TCR. OTII cells that had been co-cultured with OVA tumour-derived CAFs showed increased pCD3ζ (Figure 4c).

FIGURE 3

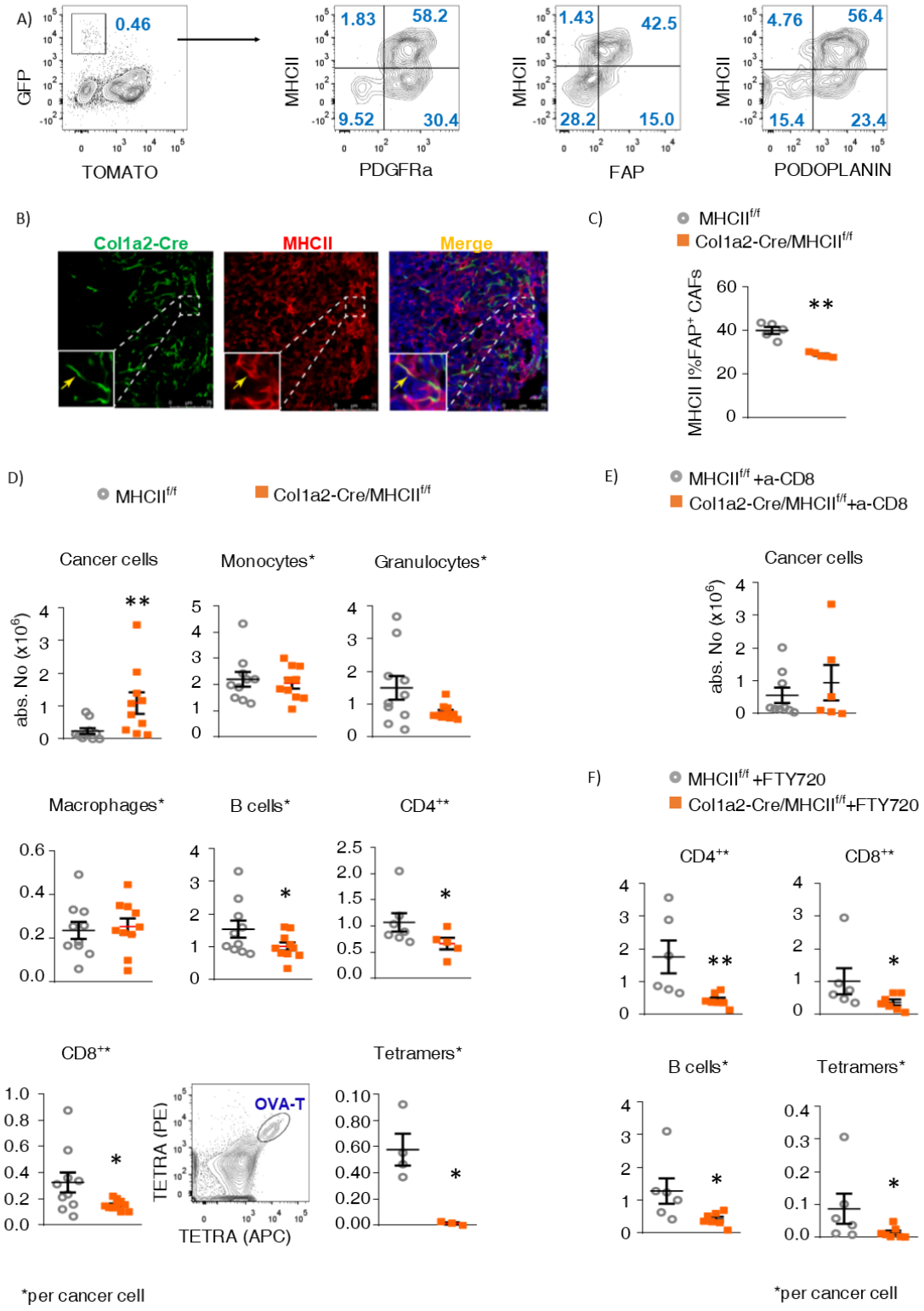

Figure 3: CAF-specific ablation of MHC Class II facilitates tumor escape. A) *Representative FACS plots data showing expression scheme of fibroblast markers and MHCII in GFP$^+$ cells of LLC lung tumors of*

Col1a2 CreER^{+}I-Ab$^{fl/fl}$ROSA$^{mT/mG}$ mice (n=2, from 2 independent experiments). ***B)*** *Confocal images from IF staining of a tumor section using MHCII antibody. Sections from 2 different mice were stained. Arrow is pointing to example of MHCII^{+}GFP^{+} cells.* ***C)*** *MHCII expression in FAP^{+} CAFs from Col1a2 CreER^{+}I-Ab$^{fl/fl}$ versus Col1a2 CreER^{-}I-Ab$^{fl/fl}$ mice (representative data from 5 independent experiments n=3-5 per group, Mann-Whitney test).* ***D)*** *Quantitative FACS data of tumors from Col1a2 CreER^{+}I-Ab$^{fl/fl}$ versus Col1a2 CreER^{-}I-Ab$^{fl/fl}$ mice showing numbers of cancer cells, immune cells and ovalbumin-specific (tetramer^{+}) intratumoral CD8^{+} T cells (cumulative data from 2 independent experiments n=3-7 per group, Mann-Whitney test).* ***E)*** *Numbers of tumor cancer cells in Col1a2 CreER^{+}I-Ab$^{fl/fl}$ versus Col1a2 CreER^{-}I-Ab$^{fl/fl}$ mice treated with CD8 T cell depleting antibodies every 3 days, starting 1-day prior inoculation of LLC cells (cumulative data from 2 independent experiments, n=3-6 per group, Mann-Whitney test).* ***F)*** *Quantitative FACS data of CD4^{+}, CD8^{+}, B- and ovalbumin-specific (tetramer^{+}) intratumoral CD8^{+} T cells from Col1a2 CreER+I-Abfl/fl versus Col1a2 CreER-I-Abfl/fl mice treated with FTY720 for 5 consecutive days, starting 7-days after inoculation of LLC cells (n=6-7 per group from 2 independent experiments, Mann-Whitney test).*

These data suggested that MHCIIp-TCR binding induced by CAFs in vivo preserved CD4^{+} T cells functional and proliferating inside tumours. To measure proliferation of cancer antigen–specific CD4^{+} T cells we labeled OTII cells with a proliferation dye and adoptively transferred them in mice bearing OVA-LLC tumours. FACS analysis of intratumoral OTII cells showed a slower proliferation rate in MHCII conditional knockout versus control mice (Figure 4d). To analyze anti-tumour function of OVA-specific T cells, we purified CD4^{+} T cells from OVA-LLC^{mCherry} lung tumours and stimulated them with mature OVA-loaded CD11c^{+} cells. A smaller percentage of CD4^{+} T cells from Col1a2 CreER^{+}I-Ab-$^{fl/fl}$ mice versus Col1a2 CreER^{-}I-Ab-$^{fl/fl}$ mice responded to CD11c^{OVA} versus CD11c by increasing expression of the cytotoxic protein granzyme B (Figure 4e). Taken together, the results described above suggest that MHCIIp-TCR binding between CAFs and CD4^{+} T cells is required to sustain the numbers and activity of CD4^{+} T cells inside tumours.

We next assessed whether the above data could be extrapolated in human cancer. Spatial heterogeneity of T cell clones suggests regional activation by neighboring APCs that present their cognate antigens[11]. Confocal imaging suggested that T cells preferentially localize in MHCII^{+} CAF dense zones (Figure 4f). We reasoned that human CAFs directly presented MHCII antigens to antigen-specific CD4^{+} T cells. Thus, we co-cultured CD4^{+} T cells and PDGFRa^{+}FAP^{+} CAFs that had been sorted from the same tumour fragment. FACS analysis showed that approximately 1 in 10 intratumoral T cells responded to direct CAF contact by CD44 up-regulation and TCR activation and this effect was abolished with panMHCII blocking antibodies (Figure 4g).

FIGURE 4

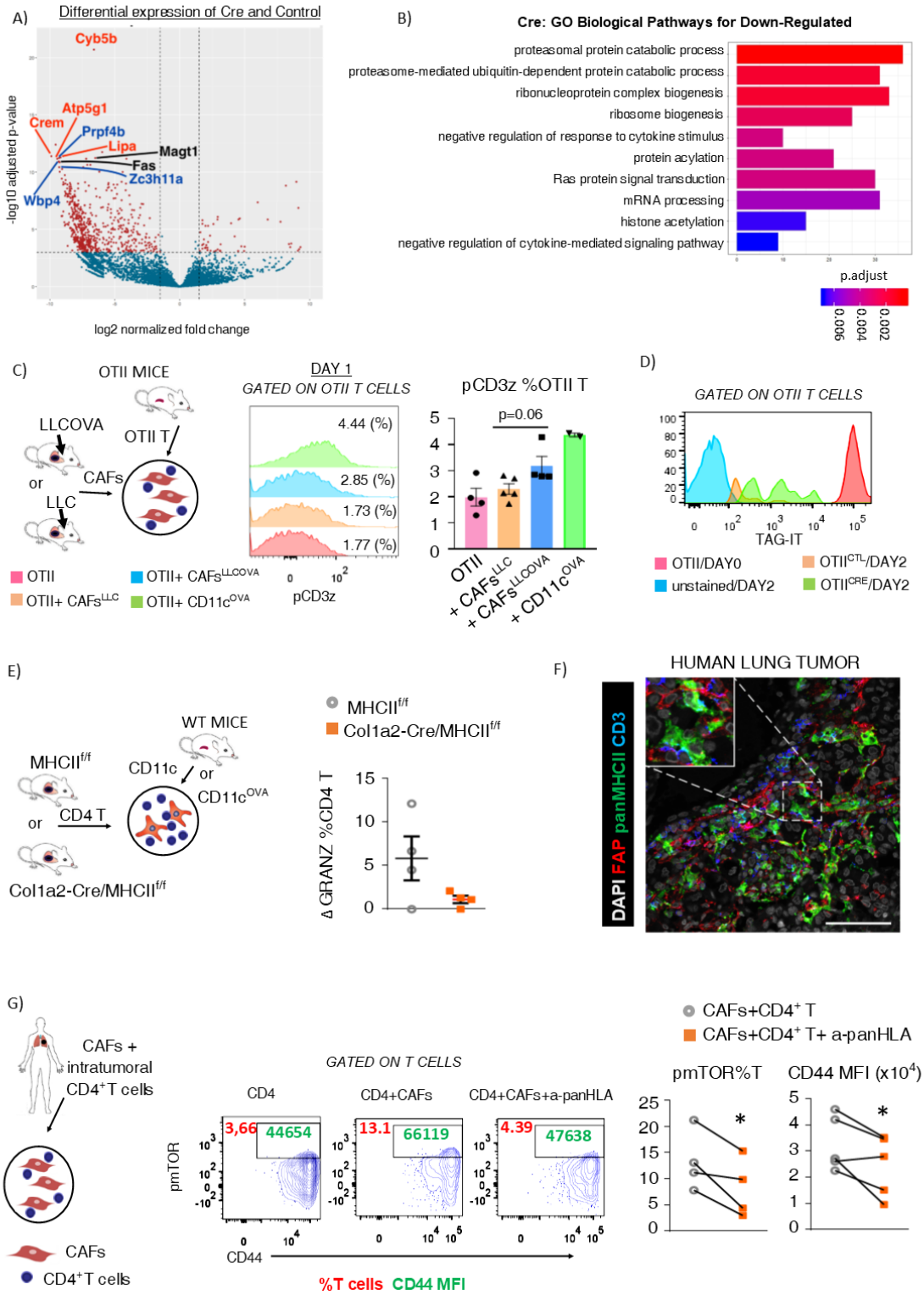

Figure 4: CAF expression of MHC-II-restricted cancer antigens stimulates tumor-specific CD4+ T cells in the TME. A) *Volcano plot representation of differential expression analysis of genes of CD4+ T cells*

sorted from tumors of the Col1a2 CreER^{+}I-Ab$^{fl/fl}$ mice (n=2) versus Col1a2 CreER^{-}I-Ab$^{fl/fl}$ mice (n=5). Red marks the genes with significantly increased (Right) or decreased (Left) expression in Col1a2 CreER^{+}I-Ab$^{fl/fl}$ (FDR<0.01). ***B)*** *Gene Ontology enrichment analysis for highly divergent genes. GO terms found over-represented by a two-tailed Fisher Exact test with a p-value below 0.05.* ***C)*** *CAFs (FS^{hi}Lin^{-} PDGFRa^{+}) were isolated from lung tumors that were expressing or not ovalbumin. Sorted cells were co-cultured with OTII T cells. Stimulation of the TCR of OTII cells was analyzed by FACS. Representative FACS histogram plots and cumulative data are shown (n=4 from 2 independent experiments, Mann-Whitney test).* ***D)*** *Histogram plots showing in vivo proliferation of OVA-specific CD4^{+} OTII T cells from tumors of Col1a2 CreER^{+}I-Ab$^{fl/fl}$ versus Col1a2 CreER^{-}I-Ab$^{fl/fl}$ mice 2 days after adoptive transfer.* ***E)*** *CD4^{+} T cells were purified from ovalbumin-expressing lung tumors of Col1a2 CreER^{+}I-Ab$^{fl/fl}$ versus Col1a2 CreER^{-}I-Ab$^{fl/fl}$ mice and co-cultured with ovalbumin-loaded mature CD11c^{+} splenocytes (CD11c^{OVA}) or mature CD11c+ splenocytes (CD11c). CD4^{+} cytotoxic responses were assessed by intracellular GranzymeB staining followed by FACS. Data are presented as % increase in granzyme expression induced by CD11c^{OVA} versus CD11c co-culture (cumulative data from 2 independent experiments, n=2 per group).* ***F)*** *IF of CD4, panMHCII and FAP in a human lung adenocarcinoma section. Arrows are pointing to CD4^{+} T cells in close contact to panMHCII^{+}FAP^{+} cells.* ***G)*** *CD4^{+} T cells and CAFs (FS^{hi}Lin^{-}PDGFRa^{+}FAP^{+}) were sorted from the same tumor fragment and co-cultured for 2 days at 1:1 (CAFs/T) ratio, in the present or absence of panMHCII blocking antibody. Stimulation of the TCR of CD4^{+} T cells (mTOR phosphorylation-pmTOR) and expression of the activation marker CD44 were analyzed by FACS. Representative FACS plots and cumulative data are shown (n=4 patients from 4 independent experiments).*

High-throughput insight into the gene expression of human antigen-presenting CAFs unveils a previously unknown role of C1q in T cell activation

Reasoning that TCR ligation in the absence of co-stimulation leads to T cell deletion or anergy, we tested whether HLA-DR^{+} primary human CAFs expressed classical co-stimulatory molecules. As reported by Tuvenson group[17] for pancreatic adenocarcinoma apCAFs, we could not detect any CD80 or CD86, while only a minor percentage of human lung cancer CAFs expressed CD40 by FACS analysis (Supplementary Figure 5a). These results were validated in murine CAFs (Supplementary Figure 5b). To generate novel hypotheses on the molecular mechanisms governing the ability of antigen-presenting CAFs to prime CD4^{+} T cells we developed a mining public single-cell RNA-sequencing data approach. To date there is no standardized computational method for characterizing gene expression levels in a binary form of “high” and “low”. MHCIIs are signature genes of dendritic cells. Thus, we re-clustered integrated lung tumor/adjacent unaffected lung RNAseq datasets of 1284 single-cells annotated as either fibroblasts (798) or cross-presenting dendritic cells (486) (E-MTAB-6149 and E-MTAB-6653, n=3 patients) via k-means

clustering (input all MHCII genes, k=3 clusters supported by Silhouette scoring), to separate fibroblasts into 2 clusters that share ($MHCII^+$) or do not share ($MHCII^-$) MHCII expression features with dendritic cells, followed by differential expression analysis (input 1717 genes, after filtering). Initial analysis showed significant up-regulation of surfactant genes in $MHCII^+$ fibroblasts (Supplementary Figure 6). Because alveolar epithelial cells are known to produce surfactant proteins and express MHCII, we concluded that clusters originally annotated as fibroblasts had been contaminated by alveolar epithelial cells. After filtering them out we were able to discern 97 $MHCII^+$ fibroblasts (76 from tumour and 21 from adjacent lung) and 999 (923 from tumour and 76 from adjacent lung) $MHCII^-$ fibroblasts (Figure 5a). Differential expression analysis revealed a remarkably small number of de-regulated genes in $MHCII^+$ versus $MHCII^-$ fibroblasts, all of which were up-regulated (Figure 5b). Among these were CD74, a polypeptide involved in the formation and transport of MHC class II, FcER1G, involved in the capture of IgE-antigen complexes and LAPTM5 and CTSS, two lysosomal enzymes, required for antigen processing. Thus our computational approach based on MHCII gene clustering, confidently identified antigen processing and presenting fibroblasts. We confirmed increased lysosomal activity and CD74 expression in $MHCII^+$ versus $MHCII^-$ primary lung tumor CAFs by FACS in an independent cohort of lung cancer patients (Supplementary Figure 8a and b).

Comparing pathway activities between $MHCII^+$ and $MHCII^-$ fibroblasts revealed enrichment in genes that are involved in immunological processes, such as increased antigen processing and presentation, increased T cell activation and leukocyte chemotaxis (Figure 5c) (Supplementary Figure 9). When contrasting SCENIC (single-cell regulatory network inference and clustering), genes regulated by KLFs (KLF6, KLF9, KLF10), AP1 (JUN, JUNB, FOS, JUND, FOSB) and the transcription factor IRF1, were highly upregulated in $MHCII^+$ versus $MHCII^-$ fibroblasts (Figure 5d). IRF1 regulates interferon-gamma induced MHCII[28,29], while AP1 and KLFs mediate cellular responses to cytokines, growth factors and oxidants[30,31], further supporting the notion that environmental cues program CAFs to acquire antigen presenting functions.

Besides MHCII and CD74, $MHCII^+$ fibroblasts over-expressed a repertoire of other immune-related molecules that could be involved in cell-to-cell interactions: TYROPB and CD47 which ligate to SIRP receptors, CD52 and ANXA1 which bind to SIGLEC10 and ALX/FPR2, respectively, and C1q which binds to cC1qR/calreticulin and gC1qR/C1qbp (Figure 5e). To identify candidate molecules in the interaction with T cells, we manually mined the literature and also applied NicheNet, a method that predicts ligand–target links between interacting cells by combining their expression data with prior knowledge. These approaches failed to identify any candidate molecule. We hypothesized that if any of these molecules possesses a previously unknown function in T cell activation, its receptor should be expressed by intratumoral $CD4^+$ T cells. The human tumour scRNAseq data that we mined included $CD4^+$ T cells. Thus, we probed expression of the receptors for TYROPB, CD52, ANXA1 and C1q on intratumoral $CD4^+$ T cells

in the aforementioned human and our own mouse bulk RNAseq data from LLC lung tumour $CD4^+$ T cells. None, but the receptor of the globular head of C1q, i.e. gC1qr/C1qbp, was found to be expressed in lung tumour $CD4^+$ T cells (Supplementary Table 1).

C1qbp is located in most cell types in the mitochondria where it is responsible to maintain transcription of mitochondrial proteins. In the cytoplasm, gC1qr/C1qbp, referred to as splicing factor-associated protein p32 acts as a regulator of RNA stability and plays a critical role in mRNA splicing. The role of C1qbp as a plasma membrane receptor on T cells has been reported[32], but is largely unexplored. We hypothesized that C1qbp activation by apCAF C1q amplified T cell activation induced by MHCIIp-TCR binding. First, we validated C1q expression by apCAFs and membrane C1qbp expression by intratumoral $CD4^+$ T cells at the protein level by FACS (Figure 5f). Then, we repeated our co-culture experiments with autologous human intratumoral $CD4^+$ T cells and $PDGFRa^+FAP^+$ CAFs in the presence of C1qbp blocking antibodies. Blocking C1qbp decreased T cell activation in $CD4^+$ T cell-CAFs co-cultures, but had no effect on T cell cultures, suggesting that it was blocking paracrine rather than autocrine C1q signaling (Figure 5g). These data support a model in which intratumoral $CD4^+$ T cells require two distinct signals from CAFs in order for activation and proliferation to occur. The first signal is provided by MHCIIp binding to the TCR. The second signal is provided by interaction of C1q with C1qbp.

DISCUSSION

The work described herein focuses on the functional role of MHCII expressing CAFs (apCAFs) in mediating anti-tumour responses using human functional ex-vivo assays and an orthotopic lung cancer model. Using MHCII conditional KO in fibroblasts and ovalbumin expressing cancer cells, we have shown and validated that apCAFs present an MHCII ovalbumin epitope on intratumoral ovalbumin-specific $CD4^+$ T cells to trigger TCR signaling. MHCII on apCAFs was required to sustain metabolically active proliferating $CD4^+$ T cells inside lung tumours and restrain tumour growth. Moreover, cancer MHCI immunity was strongly dependent on MHCII immunity. It is reasonable that MHCIIp-TCR binding by itself is insufficient to enable $CD4^+$ T-cell activation. However, murine and human apCAFs lack classical co-stimulatory molecules. Our date suggest that a second signal is provided by complement 1 q (C1q). Thus, we have convincingly shown that MHCII cancer antigen presentation by CAFs sustains functional proliferating anti-tumour $CD4^+$ T cells and unveiled a novel unconventional pathway to T cell co-stimulation.

FIGURE 5

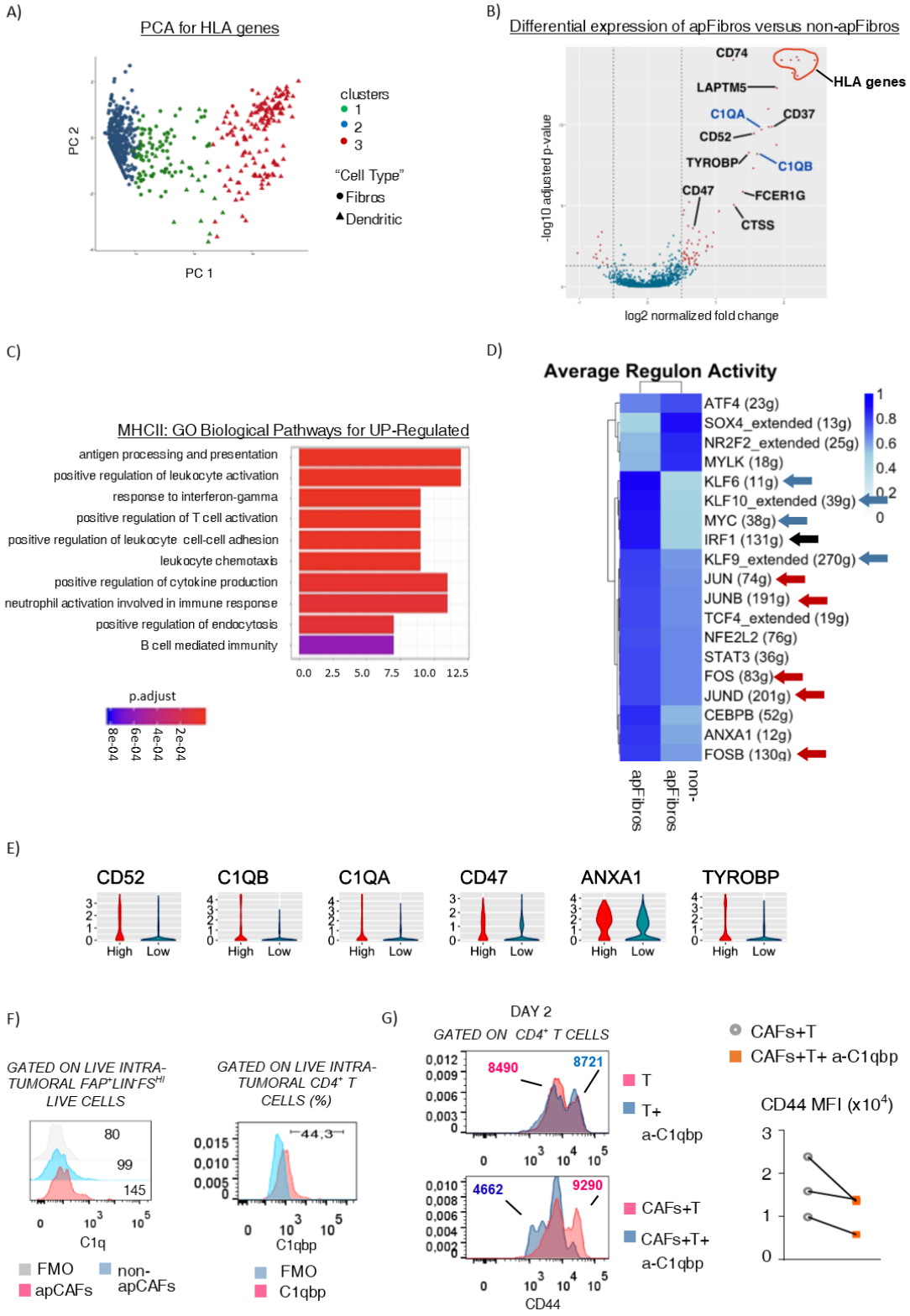

Figure 5: Transcriptional regulation and co-stimulatory function of human apCAFs. A) *Fibroblast and dendritic cell clusters in RNAseq datasets of 1265 single cells from lung tumors and adjacent lungs were*

re-clustered based on k-means (input all MHCII genes, k=3 clusters) and presented as a PCA plot, color-coded by their associated cluster (E-MTAB-6149 and E-MTAB-6653) (n=3 patients) ***B)*** *Volcano plot representation of differential expression analysis of genes of HLA^+ (n=97 cells) versus HLA^- cluster (n=999 cells). Red marks the genes with significantly increased (Right) or decreased (Left) expression in the HLA^+ cluster (FDR<0.01).* ***C)*** *Differences in pathway activities scored per cell by Gene Ontology enrichment analysis between the two clusters. Shown are GO terms found over-represented by a two-tailed Fisher Exact test with a p-value below 0.05.* ***D)*** *Heatmap of the t values of AUC scores of expression regulation by transcription factors (TFs), as estimated using SCENIC, per cluster. Shown are t values from a linear model for difference between cells from one cluster and cells from all other clusters and this for all TFs having at least one t value exceeding 6 (The top 20 factors). TFs of high biological relevance are pointed by arrows. Same colour arrows denote same family TFs.* ***E)*** *Violin plots of top up-regulated genes, showing normalized expression in HLA^+ versus HLA^- clusters.* ***F)*** *Histogram plots showing expression of C1q in human intratumoral apCAFs ($HLA\text{-}DR^+FAP^+LIN^-FS^{hi}$) and non-apCAFs ($HLA\text{-}DR^-FAP^+LIN^-FS^{hi}$) and C1qbp on intratumoral $CD4^+$ T cells (representative of n=2).* ***G)*** *$CD4^+$ T cells and CAFs ($FS^{hi}Lin^-PDGFRa^+FAP^+$) were sorted from the same tumor fragment and co-cultured for 2 days at 1:1 (CAFs/T) ratio, in the present or absence of C1qbp blocking antibody. Activation of $CD4^+$ T cells, with the activation marker CD44, was analyzed by FACS. Representative histogram plots and cumulative data (n=3 patients from independent experiments).*

The quantitative data that we got from our immunohistochemical analysis of primary human lung tumours show that apCAFs are a major constituent of the total pool of intratumoral MHCII expressing cells in most lung cancer patients. We find of particular interest that FACS analysis impressively underestimated the number of apCAFs among total MHCII expressing cells compared to immunohistochemistry. This discrepancy likely reflect disparities in dissociation efficiency of different cell types following tissue digestion, with fibroblasts being more adherent to the extracellular matrix and basement membrane than immune cells, and hence more difficult to dissociate.

The advents of single cell technologies lead to the appreciation of CAF heterogeneity and plasticity, explaining past contradictory data on their role in tumorigenesis and impact on clinical outcomes. A new subset of CAFs that express MHCII was described in pancreatic adenocarcinoma[17] and breast cancer (bioRxiv, doi.org/10.1101/2020.01.12.903039). By confirming the existence of apCAFs in human lung adenocarcinomas and squamous cell carcinomas, we provide additional evidence that apCAFs should exist in most solid tumours. Our data support a model where environmental cues, mainly IFNγ and oxidants, program CAFs to antigen-presenting cells via specific transcription factor networks, among which IRF1, KLFs and AP-1.

Using the Col1a2creER strain that specifically targets fibroblasts, we have shown MHCII expression by fibroblasts is required for optimal priming of $CD4^+$ T cells inside lung tumours and their maintenance in a metabolically active proliferating state. We have also shown that MHCII deletion affects cancer antigen specific MHCII and MHCI immunity and tumour growth. Showing an impact on MHCI immunity by targeting MHCII expression we also provide strong in vivo evidence that, as proposed by others, anti-tumour $CD8^+$ T cells are strongly dependent on MHCII antigens presented on $CD4^+$ T cells[1]. Our observations fit well with the general model for T effector cell retention at non-lymphoid tissues: initial capacity for migration depends on selectins, chemokine receptors and integrins, but persistence in situ depends on cognate MHCIIp recognition[8-10]. Three more lines of evidence support the application of this model in tumour immunity: i) stem-like T cells reside in dense antigen-presenting-cell niches within the tumour[33], ii) the distribution of T cell clones in distinct tumour regions reflects the nonsynonymous mutational load of the regions, indicating a neoantigen-driven process[11] iii) right flank tumours that differ only in one MHCII neoantigen with left flank tumours, are infiltrated by higher numbers of neoantigen-specific $CD4^+$ T cells[1].

Although co-stimulation is an established pivotal mechanism of T cell priming. Besides CD28, T cells express many other co-stimulatory receptors, some of which act independently of TCR signaling[34]. Our ex-vivo work proposes an unknown co-stimulatory pathway triggered by C1q binding on surface C1qbp. C1q is known to regulate basic metabolic processes of T cells[35-37] and has been largely disregarded as an extracellular communication signal . This is also related to the fact that the receptor of its globular head, C1qbp, has a very short intra-cytoplasmic tail and must complex with other membrane molecules to trigger intracellular signaling[38,39]. Albeit we did not look for other receptor molecules that complex with C1qbp on T cells, our data point to C1qbp as a novel T cell stimulatory receptor.

Based on our data we expect that patients with tumours with dense apCAFs will have increased numbers of endogenous T cells and better clinical outcomes. Current immunotherapeutic strategies largely focus on immune cells. Our works suggests that non-immune cells should not be disregarded as partners in cancer immunotherapies. We envisage two possible scenarios for the immunotherapeutic exploitation of apCAFs: in vivo delivery of tumour antigens in apCAFs and amplification of apCAFs niches by cellular re-programming of resident CAFs to transition to apCAFs in situ.

METHODS

Human samples and mouse models. Paired human lung tumour and macroscopically healthy lung resection specimens were obtained from patients with lung adenocarcinoma (LUAD) and squamous cell carcinoma (LUSC) at Sotiria Chest Hospital. The study was approved by the ethical committee of the Hospital and informed consent was obtained from all patients. LUADs and LUSCs were clinically scored and staged according to the International Union against Cancer (UICC) TNM staging system. The clinical and pathological characteristics of all patients included in this study are summarized (Supplementary Table 2).

Col1a2-cre/ERT,-ALPP mice (Jackson Laboratories ,ID #029235), Tg(Col6a1-cre)1Gkl (ColVI-Cre) mice (MGI:3775430), B6.129X1-Twist2tm1.1(cre)Dor/J (Twist2-Cre) mice (Jackson Laboratories ,ID # 008712), mTmG mice (Jackson Laboratories ,ID #007576),IL12 p35 knockout (Jackson Laboratories ,ID #002691) and IL12 p40 knockout (Jackson Laboratories ,ID # 002693) mice were provided by G. Kollias, (BSRC Al. Fleming) ,OTII mice (Jackson Laboratories ,ID #004194) by V. Andreakos (BRFAA) and IFNgR (Jackson Laboratories ,ID #003288) and IFNg knockout mice (Jackson Laboratories ,ID #002287) from J.P. Gorvel (CIML). For MHCII deletion in fibroblasts the Col1a2-cre/ERT,-ALPP mice were crossed to B6.129X1-H2-Ab1tm1Koni/J (I-AB-flox) mice (Jackson Laboratories, ID #013181) that possess a loxP-flanked neo cassette upstream of exon 1, and a single loxP site downstream of exon 1 of the H2-Ab1 locus. For T cell responses against ovalbumin-expressing cancer cells, OTII mice that express the mouse alpha-chain and beta-chain T cell receptor that pairs with the CD4 co-receptor and is specific for the chicken ovalbumin 323-339 peptide in the context of I-Ab were crossed to Rag1 knockout mice. For reporter studies Col1a2-cre, Tg(Col6a1-cre)1Gkl (ColVI-Cre) and B6.129X1-Twist2tm1.1(cre)Dor/J (Twist2-Cre) were crossed to mTmG mice. Gender-matched, over 8-week-old mice were used for all studies. All mice were housed under standard special pathogen-free conditions at BSRC Alexander Fleming. All animal procedures were approved by the Veterinary Administration Bureau, Prefecture of Athens, Greece under compliance to the national law and the EU Directives and performed in accordance with the guidance of the Institutional Animal Care and Use Committee of BSRC Al. Fleming.

For the orthotopic lung cancer model, mice were anesthetized via i.p. injection with xylazine and ketamine. Cancer cells (2×10^5) resuspended in 50 ul DMEM (Gibco) and enriched with 20% growth-factor reduced extracellular matrix (Matrigel, BD Biosciences) were intrapleurally injected in the lung parenchyma of mice using a 29G needle (BD Biosciences). For the metastatic model, mice were injected i.v. (intravenously) with 4×10^5 B16 cells in 100 μl DMEM medium.

Monoclonal antibody aCD8/2.43, produced as described previously[43] and administered intraperitonealy (i.p.) 2 days before tumor implantation and continuing 3 times per week for the duration of the study

(150ug/mouse). FTY720 (Cayman Chemicals, USA) was administered i.p. for 5 consecutive days, starting on day 7 after tumor cell transplantation at 20 mg per mouse.

To assess in vivo proliferation, 10^4 cells in vitro expanded OTII T cells were stained with Tag-it Violet Proliferation and Cell Tracking Dye, as per manufacturer's instructions (Biolegend) and adoptively transferred i.v. in lung tumor-bearing mice 2 days prior to euthanasia.

Cell lines. The Lewis Lung Carcinoma cell line (LLC) was obtained from American Type Collection Cultures (Manassas, VA). Platinum-E packaging cells were transfected with the retroviral plasmid MIGR1-OVA-IRES-mCherry FP and viral supernatants infected LLC cells to create ovalbumin-mCherry expressing LLC cells (LLCOVA), as described[43]. The 2.43 ATCC-TIB-210 hybridoma cell line, expressing the monoclonal antibody against Lyt-2.2, was purchased from ATCC (Rockville, MD). The C57BL/6-derived urethane-induced lung adenocarcinoma CULA cell line was provided by G. Stathopoulos (University of Patras) and the C57BL/6-derivered melanoma cell line B16F10 by V. Kostourou (BSRC Al. Fleming). Cells were maintained in Dulbecco's Modified Eagle Medium, containing 10% heat-inactivated FBS, 1% L-glutamine and 1% penicillin/streptomycin (Gibco).

Sample preparation and staining. Human and murine tissue specimens were perfused with PBS and cut into pieces. Minced samples were immediately processed or cryopreserved using BioCool (SP Scientific) in Recovery Cell Culture Freezing Medium (Gibco, Cat. No.12648-010) enriched with 10% DMSO. Human and mouse tumour and lung tissue fragments were enzymatically digested in 10% FBS/HBSS (Gibco) using Collagenase IV (Sigma-Aldrich, 1 mg/ml, Cat. No.C7657), Dispase II (Roche, 1 mg/ml, Cat. No.SCM133) and Dnase I (Sigma-Aldrich, 0.09 mg/ml, Cat. No DN25) for 1 hour at 37°C with agitation. Murine lymph nodes were digested 10% FBS/HBSS using Collagenase P (Sigma-Aldrich, 1 mg/ml, Cat. No. 11 249 002 001), Dispase II (Roche, 1 mg/ml,) and Dnase I (Sigma-Aldrich, 0.09 mg/ml,) for 1 hour at 37°C with agitation. Human cells were passed through a 100 μm cell strainer and murine cells were passed through a 70 μm cell strainer. Cells were washed with FACS buffer (2%FBS/PBS/1.5mM EDTA), centrifuged and re-suspended in FACS buffer. Non-specific binding was blocked by incubating cells with human anti-Fc Receptor antibodies (TrueStain, Biolegend, Cat. No. 101320) or anti-mouse CD16/32 Fc block (Biolegend, Cat. No. 101310).

Staining of human tissue was performed with the following antibodies (all from Biolegend, unless otherwise stated): CD45-PE, (Cat. No. 304007), CD31-PE, (Cat. No. 303105), EpCAM-PE, (Cat. No. 324205), FAP-Alexa700 (R&D Biosystems, Cat. No. MAB3715), Podoplanin APC-Fire 750, (Cat. No. 337023), CD140a (PDGFRa)-PE-Cy7, (Cat. No. 323507), CD29-FITC, (Invitrogen Cat. No. 11-0291-82), CD40-BV421, (Cat. No. 334331), CD80-BV510, (Cat. No. 305233), CD86-APC, (BD,Cat. No. 555660), CD45-PE, (Cat.

No. 304007), CD8-PERCP-Cy5.5, (Cat. No. 301031), CD5-BV521, (Cat. No. 300625), HLA-DR-BV785, (Cat. No. 307641), C1q (Biorad, Cat. No. AHP033), GC1qR (Abcam, Cat. No. ab24733) and CD44-APC (Biolegend, Cat. No. 103011) for 30 minutes at 4°C. Sytox-Green viability dye (ThermoScientific, Cat. No. S7020), Zombie NIR (Biolegend, Cat. No. 423105), Zombie Violet (Biolegend, Cat. No. 423113) was used to exclude dead cells.

For labelling of acidic organelles in human cells, Lysotracker Green DND-26 (ThermoScientific, Cat. No. L7526), was used following manufacturers' instructions. In brief, tissue cells were stained with Lysotracker green (50nM) for 1 hour at 37°C. Cells were then washed in PBS and stained.

Murine cells were stained with the following antibodies (all from Biolegend, unless otherwise stated): CD40-PE (BD Pharmigen, Cat. No. 553791), CD80-PERCP-Cy5.5 (Cat. No. 104721), CD86-FITC (BD Pharmigen, Cat. No. 09274), CD45-APC-CY7 (Cat. No. 103115), CD3-PE-CY7 (eBioscience, Cat. No. 25-0031-82), F480-PE (eBioscience, Cat. No. 12-4801-82), Ly6G-APC (Cat. No. 127617), Ly6C-FITC (BD Pharmigen, Cat. No. 553104), B220-PERCP (eBioscience, Cat. No. 45-0452-82), CD8-PERCP (Cat. No. 126610), CD4-FITC (BD Pharmigen, Cat. No. 553651), CD45-Alexa700 (Cat. No. 123128), CD31-Alexa700 (Cat. No. 102443), EpCAM-Alexa700 (Cat. No. 334331), CD140a (PDGFRa)-PE (Cat. No. 334331) or BV785 (Cat. No. 118239), Podoplanin-PE Cy7 (Cat. No. 127412), MHCII-APC-Cy7 (Cat. No.107627), FAP (Abcam, Cat. No. ab28244), and A647-anti-rabbit (Invitrogen, Cat. No. A21244) secondary antibody. Tetramers SIINFEKL-PE and SIINFEKL-APC were provided by NIH. Sytox-Green viability dye (ThermoScientific, Cat. No.S7020), Zombie NIR (Biolegend, Cat. No. 423105), Zombie Violet (Biolegend, Cat. No. 423113) or BD Horizon, Fixable, Viabilility, Stain 700 (BD Pharmigen, Cat. No. 564997) was used to exclude dead cells.

For intracellular staining, cells were fixed and permeabilised using the Intracellular Fixation & Permeabilization Buffer Set (eBioscience, Cat. No. 88-8823-88), followed by staining for human samples with PAN-Cytokeratin-PE (Sigma, Cat. No. SAB4700668), Vimentin-Alexa Fluor 674 (Abcam, Cat. No. ab194719), a-Sma-FITC (Sigma, Cat. No. F3777), CD74 PERCP-CY5.5 (Cat. No. 357607) and Alexa Fluor 647-anti-mouse (Invitrogen, Cat. No.A21235) secondary antibody. For murine samples granzymeB (Biolegend, Cat. No. 372207), anti-mCherry-APC (Invitrogen, Cat. No. M11241), a-Sma-FITC (Sigma, Cat. No. F3777) and Vimentin-Alexa Fluor 674 (Abcam, Cat. No. ab194719) were used.

For intracellular staining of phosphorylated proteins, cells were fixed and permeabilised using the Intracellular Fixation & Permeabilization Buffer Set (eBioscience, Cat. No. 88-8823-88) as per manufaturers' recommendations for detection of intracellular phosphorylated proteins, followed by staining with pmTor-PE-Cy7 (eBiosciences, Cat. No. 25-9718-42) and CD247-Al647 (pY142, CD3zeta) (BD Pharmigen, Cat. No. 558489).

Functional ex-vivo assays. For human immunological assays, CAFs, CD11c$^+$ cells and CD4$^+$ T cells were sorted from the same tumour fragment. CAFs were sorted as CD45$^-$CD31$^-$EPCAM$^-$FAP$^+$PDGFRa$^+$ cells. To preserve functional TCRs, CD4$^+$ T cells were sorted as CD45$^+$CD5$^+$CD8$^-$. CAFs or CD11c$^+$ cells were co-cultured with CD4$^+$ T cells at a 2:1 ratio in the presence or absence of pan-HLA blocking antibody (Biolegend, Cat. No.361702) or C1qbp blocking antibody (anti-GC1q R antibody [60.11] (Abcam, Cat. No. ab24733) for 1-2 days.

Fur murine immunological assays: For murine co-cultures CAFs were sorted as CD45$^-$CD31$^-$EPCAM$^-$, mCherry$^-$, PDGFRa$^+$ cells. Untouched CD4$^+$ T cells were sorted from splenocytes of OT-II$^{+/+}$/Rag1 KO mice as negative for TER-119-APC (eBioscience, Cat. No.17-5921-82), CD105-APC (Biolegend, Cat. No.120414), NK1.1-APC (Biolegend, Cat. No.108719), B220-PE (BD Pharmigen, Cat. No.553089), MHCII-APC (eBioscience, Cat. No.17-5320-82), CD11b-PE (BD Pharmigen, Cat. No.557397), CD11c-PE (BD Pharmigen, Cat. No. 553802). For in vitro expansion, OTII cells were cultured for 5 days in a-CD3e coated plates (Biolegend, Cat. No. 100339, 5ug/ml) with complete RPMI (10%FBS, 1% Pen/Strep, 50uM b-mercaptoethanol) supplemented with soluble a-CD28 (Biolegend, Cat. No. 102115, 1ug/ml) and mIL-2 (50U/ml, Miltenyi Biotech). CAFs cells were co-cultured with CD4$^+$ T cells in 96-well round-bottom tissue culture plates at a 2:1 ratio. For splenic CD11c$^+$ cells and intratumoral CD4$^+$ T cells co-cultures, untouched intratumoral CD8$^-$ -PerCP (BD Pharmigen, Cat. No.553036) CD4$^+$T cells were sorted as above, among lymphocytes (FSC-A, SSC-A low cells). To enrich for CD11c$^+$ cells, spleen cells were stained with CD11c-PE conjugated antibody and sorted magnetically with anti-PE-conjugated magnetic beads (Miltenyi) according to manufacturer's instructions. Cells eluted from the column were >87% CD11c$^+$. CD11c$^+$ cells were cultured with intratumoral CD4$^+$ T cells in 96-well round-bottom tissue culture plates (ratio 2:1) with or without OVA protein (500μg/ml, Invivogen) in the presence of polyI:C (100 ng/ml, Invivogen) and mouse IL-2 (50U/ml). Cells were harvested after 7 days of co-culture and T cells analysed by FACS.

For murine 3D CAF cultures, FACS sorted CAFs were resuspended in liquified Matrigel (354254, Corning) at 4oC. Approximately 30.000cells/well were seeded in a 25ul drop of Matrigel in the centre of wells of a 48-well tissue culture plate. The matrix was allowed to set for 15 minutes at 37oC before adding 400ul RPMI 1640 medium containing 10% FBS 1% Pen/Strep into each well. At day 5 of culture, RPMI medium was replaced with fresh RPMI supplemented with 30% healthy lung or tumor lung homogenate and/or the following cytokines or neutralizing antibodies: rIFN-γ (20ng/ml, Peprotech), sulforaphan (SFN, 40uM, Sigma-Aldrich), N-acetyl-L-cysteine (NAC, 3mM, Sigma-Aldrich), anti-IFN-γ (10μg/ml, Biolegend, Cat. No. 505705). To obtain tissue homogenates, tumors or healthy lungs were excised, weighed and homogenized in PBS (30%, weight/volume) on ice. Samples were centrifuged at 13000rpm for 10 min at 4oC and supernatants were added in wells containing matrigel encapsulated cells.

Flow cytometry. FACS analysis or sorting was performed using FACSCANTO II (BD Biosciences) or BD FACSARIA III (BD Biosciences) and data were analyzed using Flowjo software. For calculation of absolute numbers of tumor cells (burden) or immune cells, counting beads (123Count eBeads, ThermoScientific) were used. Briefly, a known volume of counting beads was added to the same known volume of stained cells. The beads were counted along with cells. The absolute count of the cell population (A) was obtained by dividing the number of positive cell events (X) by the number of bead events (Y) and then multiplying by the bead concentration (N/V, where N = number of beads per test and V = test volume). $A = X/Y \times N/V$.

Immunohistochemistry/ Immunofluorescence

For mouse studies, lungs were excised from healthy and tumor bearing mice and fixed in 4% freshly prepared paraformaldehyde for 14-18 hours at 4o C. After fixation and incubation in 30% sucrose samples were embedded in O.C.T (VWR Cat. 361603E), then sectioned (10μm in thickness) onto SuperFrost Plus™ microscope slides (Thermo Scientific™). Slides were washed using PBS followed by 1 hour incubation in blocking solution (1% BSA + 0,1% Saponin in PBS). Then sections were incubated with primary antibodies Anti-Mouse MHC-II 1:250 (EBiosciences 14-5321-81) and Anti-Mouse Podoplanin eFluor® 660 1:500 (EBiosciences 50-5381-82) diluted with BSA 1% in PBS overnight at 4o C. After rinsing with PBS + 0,1% Saponin, sections were incubated with secondary antibody for MHC-II (Goat anti-Rat IgG (H+L) Alexa Fluor 594™) for 1 hour at room temperature. Nuclei were stained with DAPI and slides were mounted using Fluoroshield™ mounting media (Sigma F6182). Images were acquired with a TCS SP8X White Light Laser confocal system (Leica).

For IHC and IF stainings of human formalin-fixed paraffin-embedded (FFPE) tissues, three-micron thick sections on charged glass slides were deparaffinized in xylene and rehydrated in a graded series of ethanol's. Sections were incubated for antigen retrieval (Tris EDTA ph9) for 20 minutes in the microwave and let cool down for 20 minutes at room temperature. For IHC, endogenous peroxidase was blocked by applying UltraVision Hydrogen Peroxide Block (ThermoScientific) for 15 min. Nonspecific protein-binding sites were blocked with UltraVision Protein Block (ThermoScientific) for 5 minutes. Sections were stained with anti-FAP (Abcam ab207178) 1:250 or anti-HLA-DR+DP+DQ (Abcam ab7856) 1:200 overnight at 4o C. Immunodetection was performed using UltraVision Quanto Detection System HRP Polymer DAB (ThermoScientific) according to the manufacturer's instructions. 3,3′diaminobenzidine Quanto Chromogen (ThermoScientific) was used as chromogen. Slides were counterstained with hematoxylin. For IF, nonspecific protein-binding sites were blocked with 1%BSA. Then sections were incubated with anti-FAP (Abcam ab207178) 1:250 overnight at 4o C. After secondary antibody staining (Goat anti-Rabbit IgG Alexa

Fluor 594 Catalog # R37117), sections were washed 10 times and incubated for 30 minutes with AffiniPure Fab Fragment Donkey Anti-Rabbit IgG (H+L). Then sections were incubated with anti-HLA DR+DP+DQ (Abcam ab7856) 1:200 and anti-CD4 (Abcam ab133616) 1:100 overnight at 4o C. After rinsing, sections were incubated with secondary antibodies (Goat anti-Mouse IgG Alexa Fluor 647 Catalog # A-21235 and Goat anti-Rabbit IgG, Alexa Fluor 488 Catalog # A-11008). Nuclei were stained with DAPI and slides were mounted using Fluoroshield™ mounting media (Sigma F6182). Images were acquired with a TCS SP8X White Light Laser confocal system (Leica).

RNA preparation and qPCR. Intratumoral $CD4^+$ T cells were FACS sorted in RL buffer. RNA was extracted using the Nucleospin RNA kit (Macherey Nagel), followed by cDNA synthesis using Superscript II reverse-transcriptase (Thermo Fisher Scientific), as per manufaturers' instructions. For quantification of gene expression, qRT-PCR of template RNA was performed in duplicate on a CFX96 Realtime System (Biorad) using Taqman Gene Expression MasterMix and Assays (Applied Biosystems). Transcript levels of ATP5G1, RIOX2, FAS and WBP4 were determined relative to GAPDH reference gene, using the ΔΔCt method. Taqman probes were: ATP5G1 Mm02601506_g1, RIOX2 Mm00465992_m1, WBP4 Mm01324202_m1, FAS Mm01204974_m1 and GAPDH Mm9999915_g1.

Identification of human antigen-presenting fibroblasts in single cell RNA sequencing datasets. We collected processed data of publicly available paired human lung tumour and healthy lung scRNA-seq datasets (E-MTAB-6149 and E-MTAB-6653). The log2cpm values of the 22180 ensembl gene IDs were used. The transition from the raw sequence read data to the gene expression table can be found in the original publication by Lambrechts et al[40]. Processed cells annotated as fibroblasts were included in the analysis. Patient #1 was excluded from the analysis because of the small number of Fibroblasts (9 cells). Patient #2 was excluded from the analysis because of the small number of healthy Fibroblasts and dendritic cells (5 and 11 cells respectively). Only fibroblasts of patients #3, #4 and #5 were analyzed (n=643, 155 and 486, respectively). During the exploratory analysis of the dataset we discovered that cells expressing high levels of Surfactant Protein C (SFTPC) were over-represented among MHCII expressing fibroblasts (Supplementary Figure 6). Because alveolar cells are known to express MHCII[41], cells with SFPTC expression value >0 were considered alveolar cells and removed from the analysis. After this filtering, we proceeded to the analysis of 1096 fibroblasts.

To identify $MHCII^+$ and $MHCII^-$ fibroblasts, cells annotated as cross-presenting dendritic cells in the same dataset were used as positive control for MHCII expression. The 9 MHCII genes (HLA-DRA,HLA-DRB5, HLA-DRB1, HLA-DQA1, HLA-DQA2, HLA-DQB1, HLA-DQB2, HLA-DPA1, HLA-DPB1) were used for re-clustering fibroblasts and dendritic cells with kmeans function of cluster R package with k=3 (tuned

for k=3:10), supported by mean Silhouette information scoring, calculated by silhouette function of cluster R package, (Supplementary Image 6). This resulted in the splitting of the cells into 3 groups (low, middle and high MHCII expression). Fibroblasts of middle and high groups were considered as $MHCII^+$ fibroblasts (97 cells), while those of low group as $MHCII^-$ fibroblasts (999 cells). Relative numbers of $MHCII^+$ and $MHCII^-$ fibroblasts were in accordance to those obtained by FACS analysis of independent patients (Figure 2a). Distributions of the expressions of the MHCII genes between $MHCII^+$ and $MHCII^-$ fibroblasts were statistically different, supported by Welch two Sample t-test (Supplementary Image 10). In addition, differential gene expression analysis between HLA^+ and HLA^- fibroblasts with all genes as input, showed significantly up-regulated HLA genes in cells annotated as $MHCII^+$ fibroblasts. Overall, these findings testify to the biological relevance of our bioinformatics approach to identify MHCII expressing fibroblasts. Gene IDs that had zero expression in all fibroblasts were removed from the analysis (16877 IDs were kept). 15487 out of them were successfully translated into gene names using the biomaRt R package. After the characterisation of $MHCII^+$ and $MHCII^-$ fibroblasts, genes with non-zero expression values in more than 25% of each group were kept (1603 genes for apCAFs and 1402 genes for non-apCAFs). The union of the both lists was considered as the list of the genes that are expressed in at least one group. This resulted in 1717 genes.

Differential expression and pathway analysis of human antigen-presenting fibroblasts. To identify the differential expressed genes between the $MHCII^+$ and $MHCII^-$ fibroblasts we applied 3 different tools (monocle2, DEsingle and EMDomics). The results of monocle2 were excluded, since it returned 1614 DE genes. The results of EMDomics were used only for comparison purposes, since the method does not return normalized fold change values. DEsingle R package was used with default parameters. Setting as threshold for the adjusted p-value the value 0.05 and as threshold for the log Fold Change +- 0.5, the method returned 78 genes, out of which the 12 were down regulated in $MHCII^+$ fibroblasts and the rest 66 were up regulated. All 78 genes that were identified as deregulated by DEsingle were also found deregulated by EMDomics.
GO and KEGG enrichment analysis for apCAFs was done based on all 66 upregulated genes. The clusterProfiler R package was utilized. Functions enrichKEGG and enrichGO of the package were used with pvalue and qvalue cut offs equal to 0.05 and 0.10 respectively. No KEGG pathway was identified as enriched, while 320 GO terms were found enriched with adjusted pvalue > 0.05. The same analysis was performed for the 12 down-regulated genes, but no term was returned as significantly enriched.
SCENIC was run as originally described[42], using the 20-thousand motifs database for RcisTarget and GRNboost (SCENIC version 1.1.2.2, which AUCell and RcisTarget updated in January 2019; with RcisTarget.hg19.motifDatabases.20k). The input matrix was the normalized expression matrix of 1097 CAFs with the 1717 genes passed after the splitting process.

The open source R implementation of NicheNet was applied aiming on identifying the ligands between the MHCII^{+} fibroblasts (sender) and CD4^{+} Tcells (receiver) in the E-MTAB-6149 and E-MTAB-6653 datasets[40]. 625 genes were filtered as being expressed in the CD4^{+} T cell cluster. None of the 1717 filtered genes of MHCII^{+} fibroblasts was identified as regulator.

Bullk mouse RNA sequencing data acquisition, processing and analysis. Intratumoral CD4^{+} T cells from Col1a2 CreER^{+}I-Ab-$^{fl/fl}$ and I-Ab-$^{fl/fl}$ mice were FACS sorted as described above. Total RNA was isolated by using NucleoSpin RNA (Macherey-Nagel) omitting carrier RNA. Treatment with DNAse I was performed to remove all traces of DNA. RNA integrity was assessed on an Agilent Bioanalyzer RNA 6000 Pico Chip. Quality of FASTQ files, obtained after Ion Proton sequencing, was assessed using FastQC, following the software recommendations. Alignment of sequencing reads to reference genome was performed using the software HISAT2 (version 2.1.0) with the genome reference version mm10. The raw bam files were summarized to read counts table using FeatureCounts (version 1.6.0) and the gene annotation file mus_musculus.grcm38.92.gtf of Ensembl database. The resulting gene counts table was subjected to differential expression analysis (DEA) using the R package DESeq2. DEA thresholds were set for adjusted pvalue equal to 0.05 and for logFC +-1.5, returning 726 down-regulated and 54 up-regulated genes. GO and KEGG enrichment analysis was applied, as described for MHCII+ fibroblasts. 627 GO terms were found enriched for the down-regulated genes.

Statistics and reproducibility. No statistical method was used to predetermine sample sizes. For all analysis, the integrated cells of 3 patients were used. For the G-squared tests of independence the g2Test_univariate function of Rfast R package was used. The p-value was calculated only for the upper tail through the pchisq function of the same package. The Pearson correlation values were calculated with cor base R function.

Visualization. PCA was performed using the prcomp base R function, with centering but no scaling. Box plots were generated using the ggplot2 R package and default parameters. Hence, the boxes span the interquartile range (IQR; from the 25th to the 75th percentiles), with the centerline corresponding to the median. Lower whiskers represent the data minimum or the 25th percentile minus 1.5 × IQR, whichever is greater. Upper whiskers represent the data maximum or the 75th percentile plus 1.5 × IQR (lower), whichever is lower. Violin plots were generated using the geom_violin function of ggplot2 R package, with default parameters. Volcano plots were generated using the geom_point function of ggplot2 R package. GO terms bar plots were generated using the barplot base R function with dropping. Heatmaps were generated using the pheatmap function of pheatmap R package.

Acknowledgments

We would like to thank George Kollias for helpful insights and discussions. We acknowledge George Kollias, Vassiliki Koliaraki, Evangelos Andreakos, Jean-Pierre Gorvel, and George Stathopoulos for sharing mouse models, cell lines and protocols. The NIH Tetramer Core Facility for SIINFEKL tetramers. We thank the InfrafrontierGR Infrastructure (co-funded by GR/EU, NSRF 2014-2020, ERDF, MIS 5002135) for providing mouse facilities, as well as flow cytometry, transgenesis and gene targeting. We also thank the BSRC "Al. Fleming" imaging facility, and genomics facility. MT is supported by a Stavros Niarchos Foundation (SNF) Startup Grant, a Hellenic Foundation for Research and Innovation Starting Grant (HFRI-1289) and a "Fondation Santé" research grant.

REFERENCES

1. Alspach, E.*, et al.* MHC-II neoantigens shape tumour immunity and response to immunotherapy. *Nature* **574**, 696-701 (2019).
2. Kagamu, H.*, et al.* CD4(+) T-cell Immunity in the Peripheral Blood Correlates with Response to Anti-PD-1 Therapy. *Cancer immunology research* **8**, 334-344 (2020).
3. Spitzer, M.H.*, et al.* Systemic Immunity Is Required for Effective Cancer Immunotherapy. *Cell* **168**, 487-502 e415 (2017).
4. Zander, R.*, et al.* CD4(+) T Cell Help Is Required for the Formation of a Cytolytic CD8(+) T Cell Subset that Protects against Chronic Infection and Cancer. *Immunity* (2019).
5. Ahrends, T.*, et al.* CD4(+) T cell help creates memory CD8(+) T cells with innate and help-independent recall capacities. *Nature communications* **10**, 5531 (2019).
6. Sledzinska, A.*, et al.* Regulatory T Cells Restrain Interleukin-2- and Blimp-1-Dependent Acquisition of Cytotoxic Function by CD4(+) T Cells. *Immunity* **52**, 151-166 e156 (2020).
7. Binnewies, M.*, et al.* Unleashing Type-2 Dendritic Cells to Drive Protective Antitumor CD4(+) T Cell Immunity. *Cell* **177**, 556-571 e516 (2019).
8. McLachlan, J.B. & Jenkins, M.K. Migration and accumulation of effector CD4+ T cells in nonlymphoid tissues. *Proceedings of the American Thoracic Society* **4**, 439-442 (2007).
9. Doebis, C.*, et al.* Accumulation and local proliferation of antigen-specific CD4+ T cells in antigen-bearing tissue. *Immunology and cell biology* **89**, 566-572 (2011).
10. Scholler, A.S., Fonnes, M., Nazerai, L., Christensen, J.P. & Thomsen, A.R. Local Antigen Encounter Is Essential for Establishing Persistent CD8(+) T-Cell Memory in the CNS. *Frontiers in immunology* **10**, 351 (2019).
11. Joshi, K.*, et al.* Spatial heterogeneity of the T cell receptor repertoire reflects the mutational landscape in lung cancer. *Nature medicine* **25**, 1549-1559 (2019).
12. Kambayashi, T. & Laufer, T.M. Atypical MHC class II-expressing antigen-presenting cells: can anything replace a dendritic cell? *Nature reviews. Immunology* **14**, 719-730 (2014).
13. Monteran, L. & Erez, N. The Dark Side of Fibroblasts: Cancer-Associated Fibroblasts as Mediators of Immunosuppression in the Tumor Microenvironment. *Frontiers in immunology* **10**, 1835 (2019).
14. Cheng, H.W.*, et al.* CCL19-producing fibroblastic stromal cells restrain lung carcinoma growth by promoting local antitumor T-cell responses. *The Journal of allergy and clinical immunology* **142**, 1257-1271 e1254 (2018).
15. Ozdemir, B.C.*, et al.* Depletion of carcinoma-associated fibroblasts and fibrosis induces immunosuppression and accelerates pancreas cancer with reduced survival. *Cancer cell* **25**, 719-734 (2014).
16. Rhim, A.D.*, et al.* Stromal elements act to restrain, rather than support, pancreatic ductal adenocarcinoma. *Cancer cell* **25**, 735-747 (2014).
17. Elyada, E.*, et al.* Cross-Species Single-Cell Analysis of Pancreatic Ductal Adenocarcinoma Reveals Antigen-Presenting Cancer-Associated Fibroblasts. *Cancer discovery* **9**, 1102-1123 (2019).
18. Wijdeven, R.H.*, et al.* Chemical and genetic control of IFNgamma-induced MHCII expression. *EMBO reports* **19**(2018).
19. Harari, O. & Liao, J.K. Inhibition of MHC II gene transcription by nitric oxide and antioxidants. *Current pharmaceutical design* **10**, 893-898 (2004).
20. Sosic, D., Richardson, J.A., Yu, K., Ornitz, D.M. & Olson, E.N. Twist regulates cytokine gene expression through a negative feedback loop that represses NF-kappaB activity. *Cell* **112**, 169-180 (2003).
21. Armaka, M.*, et al.* Mesenchymal cell targeting by TNF as a common pathogenic principle in chronic inflammatory joint and intestinal diseases. *The Journal of experimental medicine* **205**, 331-337 (2008).

22. Zheng, B., Zhang, Z., Black, C.M., de Crombrugghe, B. & Denton, C.P. Ligand-dependent genetic recombination in fibroblasts : a potentially powerful technique for investigating gene function in fibrosis. *The American journal of pathology* **160**, 1609-1617 (2002).
23. Hashimoto, K., Joshi, S.K. & Koni, P.A. A conditional null allele of the major histocompatibility IA-beta chain gene. *Genesis* **32**, 152-153 (2002).
24. Chiba, K.*, et al.* FTY720, a novel immunosuppressant, induces sequestration of circulating mature lymphocytes by acceleration of lymphocyte homing in rats. I. FTY720 selectively decreases the number of circulating mature lymphocytes by acceleration of lymphocyte homing. *Journal of immunology* **160**, 5037-5044 (1998).
25. Lukacs-Kornek, V.*, et al.* Regulated release of nitric oxide by nonhematopoietic stroma controls expansion of the activated T cell pool in lymph nodes. *Nature immunology* **12**, 1096-1104 (2011).
26. Brown, F.D.*, et al.* Fibroblastic reticular cells enhance T cell metabolism and survival via epigenetic remodeling. *Nature immunology* (2019).
27. van der Windt, G.J. & Pearce, E.L. Metabolic switching and fuel choice during T-cell differentiation and memory development. *Immunological reviews* **249**, 27-42 (2012).
28. Antonczyk, A.*, et al.* Direct Inhibition of IRF-Dependent Transcriptional Regulatory Mechanisms Associated With Disease. *Frontiers in immunology* **10**, 1176 (2019).
29. Hou, J.*, et al.* In Primitive Zebrafish, MHC Class II Expression Is Regulated by IFN-γ, IRF1, and Two Forms of CIITA. *Journal of immunology* **Mar 18.[Epub ahead of print]**(2020).
30. McConnell, B.B. & Yang, V.W. Mammalian Kruppel-like factors in health and diseases. *Physiological reviews* **90**, 1337-1381 (2010).
31. Shaulian, E. & Karin, M. AP-1 as a regulator of cell life and death. *Nature cell biology* **4**, E131-136 (2002).
32. Clarke, E.V. & Tenner, A.J. Complement modulation of T cell immune responses during homeostasis and disease. *Journal of leukocyte biology* **96**, 745-756 (2014).
33. Jansen, C.S.*, et al.* An intra-tumoral niche maintains and differentiates stem-like CD8 T cells. *Nature* **576**, 465-470 (2019).
34. Sundqvist, K.G. T Cell Co-Stimulation: Inhibition of Immunosuppression? *Frontiers in immunology* **9**, 974 (2018).
35. West, E.E., Kolev, M. & Kemper, C. Complement and the Regulation of T Cell Responses. *Annual review of immunology* **36**, 309-338 (2018).
36. Ling, G.S.*, et al.* C1q restrains autoimmunity and viral infection by regulating CD8(+) T cell metabolism. *Science* **360**, 558-563 (2018).
37. Kouser, L.*, et al.* Emerging and Novel Functions of Complement Protein C1q. *Frontiers in immunology* **6**, 317 (2015).
38. Hosszu, K.K.*, et al.* DC-SIGN, C1q, and gC1qR form a trimolecular receptor complex on the surface of monocyte-derived immature dendritic cells. *Blood* **120**, 1228-1236 (2012).
39. Shi, H., Fang, W., Liu, M. & Fu, D. Complement component 1, q subcomponent binding protein (C1QBP) in lipid rafts mediates hepatic metastasis of pancreatic cancer by regulating IGF-1/IGF-1R signaling. *International journal of cancer* **141**, 1389-1401 (2017).
40. Lambrechts, D.*, et al.* Phenotype molding of stromal cells in the lung tumor microenvironment. *Nature medicine* **24**, 1277-1289 (2018).
41. Hasegawa, K.*, et al.* Fraction of MHCII and EpCAM expression characterizes distal lung epithelial cells for alveolar type 2 cell isolation. *Respiratory research* **18**, 150 (2017).
42. Aibar, S.*, et al.* SCENIC: single-cell regulatory network inference and clustering. *Nature methods* **14**, 1083-1086 (2017).
43. Kerdidani, D., *et al.* Wnt1 silences chemokine genes in dendritic cells and induces adaptive immune resistance in lung adenocarcinoma. *Nature communications* **10**, 1405 (2019).